Asociación Argentina
de Mecánica Computacional

Mecánica Computacional Vol XLII, pp. 169-178
A. Caggiano, G. Etse, P. Folino, M. Goldschmit, M. Pucheta, M. Storti (Eds.)
J. Ballaben, D. Felix, R. Jaca (Issue eds.)
Buenos Aires, November 11-14, 2025

FINITE-ELEMENT MODELLING OF LATERALLY-CONFINED REINFORCED-CONCRETE SLABS DESIGNED WITH NBR6118:2023

Gabriel O. Garcia, Mauro V. Real and Paula M. Lazzari

Universidade Federal do Rio Grande do Sul, Programa de Pós-Graduação em Engenharia Civil. Porto Alegre, Brazil, ppgec@ppgec.ufrgs.br, https://www.ufrgs.br/ppgec/

Keywords: Compressive Membrane Action, Reinforced Concrete Slabs, Lateral Confinement, Finite Element Analysis.

Abstract. Lateral confinement arising from the continuity between adjacent floor elements triggers compressive-membrane action that can greatly enhance the strength and stiffness of solid reinforced-concrete slabs. To capture this phenomenon numerically, a three-dimensional finite-element model was developed in ANSYS using 20-node SOLID186 elements for the concrete - employing a Drucker–Prager plasticity surface with hardening, softening, and dilatancy - and embedded REINF264 elements for the discrete reinforcing bars. The model was calibrated against twelve unconfined and ten confined slab tests from the literature, reproducing ultimate loads with a mean experimental-to-numerical ratio of 0.99 and a standard deviation of 0.06. A factorial parametric study comprising 27 design cases (spans 4–6 m, fck 25–50 MPa, span-to-depth ratios $\approx$ 40–50) was then conducted to evaluate the slabs' behavior with and without membrane action: first with the edges free to expand in-plane, and subsequently with realistic restraint provided by neighboring slabs modelled as linear-elastic plates coupled to the target panel. Explicit consideration of lateral confinement nearly doubled the predicted ultimate load (average +97%) and showed an in-plane stiffness of around 120% of the slab axial stiffness, with the largest gains occurring in shorter spans and higher-strength concretes.

ISSN: 2591-3522 DOI: 10.70567/mc.v42.ocsid8471

1 INTRODUCTION

Traditional design theories for reinforced concrete (RC) slabs, such as elastic plate theory or yield-line theory, often significantly underestimate their true ultimate load-carrying capacity. This discrepancy was famously observed by Okleston (1956) during full-scale load tests on an existing building, where the floor slabs failed at loads nearly six times higher than their design values. This considerable reserve of strength is primarily attributed to a phenomenon known as compressive membrane action, or arching action.

1.1 The mechanism of compressive membrane action

Compressive membrane action results directly from the material properties of reinforced concrete and the slab's boundary conditions. As an RC slab is subjected to increasing transverse loads, it begins to crack in the tensile zones. This cracking causes the neutral axis of the cross-section to migrate towards the compression face. Consequently, tensile strains dominate a larger portion of the slab's depth, leading to a net tendency for the slab to expand laterally in its own plane (Liebenberg, 1966).

In a continuous floor system, this lateral expansion is restrained by the in-plane stiffness of surrounding structural elements like adjacent slabs and beams. This restraint induces a significant field of in-plane compressive forces within the slab. These compressive forces, acting concurrently with the bending moments, substantially enhance the slab's flexural resistance. This interaction is well-described by the moment-axial force (M-N) interaction diagram for a concrete section; a section subjected to axial compression can resist a higher bending moment before failure. The combination of the transverse load and the induced in-plane compression creates an internal arching mechanism that carries a significant portion of the load through thrust rather than pure flexure, thereby increasing both the ultimate capacity and post-cracking stiffness of the slab - as shown in Fig. 1, where case 2 has a higher axial load applied in the concrete section than case 1.

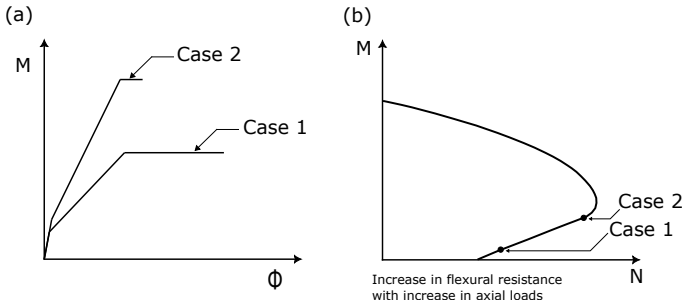

Figure 1: Generic behavior of a concrete section under combined moment (M) and axial load (N).

1.2 Research context and objectives

Following Okleston's discovery, numerous researchers have investigated this phenomenon experimentally and analytically, developing models to predict the enhanced capacity (Christiansen et al., 1963; Park, 1964; Zhu et al., 2021). However, due to the highly nonlinear behavior involved, these analytical models often rely on simplifying assumptions. The finite element method (FEM) enables a more robust study of this problem through detailed constitutive models and precise simulation of complex boundary conditions.

This paper presents a comprehensive 3D finite element model developed in ANSYS to simulate and quantify the effects of compressive membrane action in RC slabs. The primary objective is to develop a reliable numerical tool, validate it against a wide range of experimental data, and then use it to conduct a parametric study. This study aims to quantify the strength and stiffness gains in slabs designed according to the Brazilian standard NBR 6118:2023 (ABNT, 2023) when realistic lateral restraint from adjacent floor elements is considered.

This paper is structured as follows. Section 2 provides a detailed description of the finite element model, including the element types, constitutive laws for concrete and steel, and the extensive validation process. Section 3 presents the main findings from the parametric study, comparing the behavior of slabs with and without lateral confinement. Finally, Section 4 summarizes the key conclusions drawn from the numerical investigation.

2 NUMERICAL MODELING

The numerical simulations were performed using the commercial finite element software ANSYS Mechanical APDL. A fully parameterized script was developed to automate the model generation, analysis, and post-processing, facilitating the extensive validation and parametric studies.

2.1 Finite elements

To accurately capture the three-dimensional stress state, particularly the in-plane forces crucial for membrane action, a 3D modeling approach was adopted.

The concrete matrix was modeled using the SOLID186 element, a 20-node quadratic hexahedral element. Each node has three translational degrees of freedom (UX, UY, UZ). This higher-order element is well-suited for modeling curved boundaries and complex stress gradients, and it fully supports the advanced nonlinear material models required for this study.

The steel reinforcing bars were modeled using the REINF264 element. This element can be defined as a discrete fiber with a specific cross-sectional area, material, and orientation, and is embedded within a parent solid (or shell) element. The REINF264 element modifies the stiffness of the parent element to account for the reinforcement, assuming a perfect bond between the steel and the surrounding concrete (i.e., no slip is modeled). This approach allows for the modeling of complex reinforcement layouts without the need to create a conforming mesh between concrete and steel.

2.2 Constitutive material models

Accurate representation of material nonlinearity is essential for simulating the behavior of RC slabs up to failure.

The behavior of concrete was modeled using the Drucker-Prager Concrete model available in ANSYS. This is a plasticity-based model that uses a composite yield surface to handle different responses in tension and compression. The model combines a Drucker-Prager surface for the compression regime with a second surface for tension (either a Rankine criterion or another Drucker-Prager surface). For this study, the dual Drucker-Prager surface option was chosen, as it provided better numerical stability and convergence in the highly nonlinear analyses.

The post-yield behavior is modeled using a Hardening, Softening, and Dilatation (HSD) framework. A linear HSD model was adopted to define the post-cracking (softening) response in tension and the hardening and post-crushing (softening) behavior in compression, as illustrated in Fig. 2 (for further details, see ANSYS (2023)).

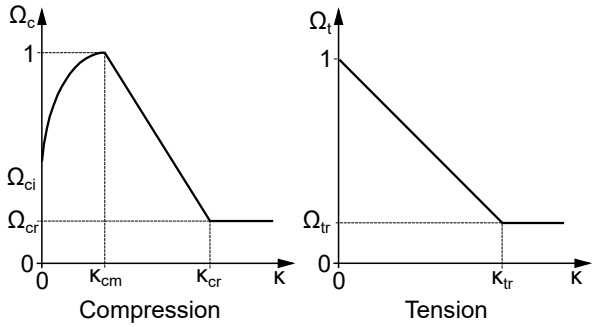

Figure 2: Ansys' Linear HSD model for concrete.

The model lacks an explicit failure criterion. Instead, structural failure is defined by the numerical solution's non-convergence due to extensive material softening, indicating the structure cannot sustain additional load.

The steel reinforcing bars were modeled using a bilinear elastoplastic model with isotropic hardening, based on the Von Mises yield criterion. This model is defined by the initial Young's modulus (E_s), the yield stress (f_y), and a tangent modulus (E_t) for the post-yield hardening branch - as illustrated in Fig. 3.

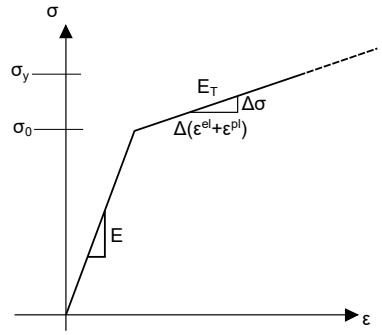

Figure 3: Bi-linear elastoplastic model used for steel reinforcement.

Parameters such as concrete's compressive strength (f_{ck}), modulus of elasticity (E_c), and tensile strength (f_t); and the steel reinforcement's yield stress (f_y), Young's modulus (E_s) and tangent modulus (E_t) were taken directly from the original experimental studies when available. When not all parameters were available, values were derived based on the recommendations of the Model Code FIB (2010).

2.3 Model validation

The numerical model was validated against the experimental results of 12 unconfined and 10 confined slabs reported in the literature. These validation simulations were designed to replicate the exact conditions of the cited experimental tests. The load was typically applied as a uniformly distributed pressure on the top surface of the slab, except for the tests by Pires (2003), where two line loads were used to match the experimental setup. The analysis was conducted statically, with the load applied incrementally until failure, which was defined by the non-convergence of the numerical solution.

2.3.1 Unconfined slabs

The unconfined slabs were modeled as simply supported. Due to symmetry, only one-quarter of each slab was discretized. Vertical displacement was restrained at the bottom nodes of the support edges, and symmetry boundary conditions were applied to the other two edges. A mesh sensitivity study found that elements approximately 10 cm in plane and 1 cm in thickness provided a good balance between accuracy and computational efficiency. The numerical model used to reproduce the experimental results is illustrated in Fig 4.

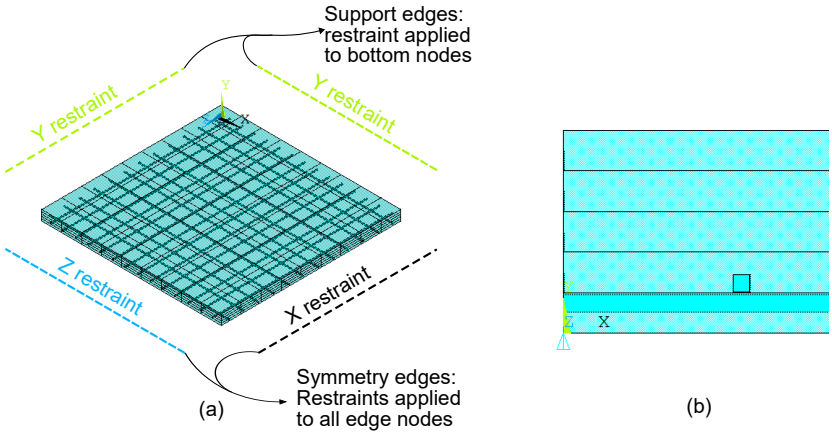

Figure 4: Boundary conditions for the quarter-model of the unconfined, simply supported slabs. (a) Isometric view (b) support edge.

Table 1 presents the validation results of the numerical model for 12 tests on unconfined slabs, along with the corresponding sources for the experimental data. The comparison includes the experimental ultimate load (Qu,exp), the numerical ultimate load (Qu,num), and the resulting ratio between these values (Qu,exp/Qu,num). As the results indicate, the model accurately predicted the ultimate load of the experimental tests, yielding an average experimental-to-numerical ratio of 0.99.

Slab	Qu,exp (kN)	Qu,num (kN)	exp/num	Error (%)	Reference
S1	124.27	123.2	1.01	0.9	
S7	116.19	123.38	0.94	5.8	Taylor et al. (1966)
S9	113.74	109.46	1.04	3.9	
L7	63.02	69.91	0.90	9.9	Geymayer and McDonald (1967)
L1	143.27	140.99	1.02	1.6	Gomes et al. (2012)
S7	65.00	59.65	1.09	9.0	Abdul-Wahab and Khalil (2000)
S8	89.72	82.44	1.09	8.8	
P1	66.94	62.61	1.07	6.9	
P2A	116.31	124.58	0.93	6.6	
P2B	114.93	124.58	0.92	7.7	Pires (2003)
P3A	119.31	124.42	0.96	4.1	
P3B	117.79	124.42	0.95	5.3	

Table 1: Validation data for unconfined slabs.

2.3.2 Confined slabs

While numerous modern numerical studies on membrane action exist (e.g., Zhu et al., 2021), comprehensive experimental data for rigidly-confined, uniformly-loaded slabs remains scarce. The foundational tests by Keenan (1969) and Rankin et al. (1991), despite their age, are still widely used as benchmarks for validating numerical models due to their detailed documentation and the difficulty and expense of replicating such large-scale experiments.

As the confined slabs were experimentally tested with rigid steel frames preventing any lateral movement, the numerical model was developed to correctly simulate this condition - by restraining both vertical and lateral displacements at all nodes along the support edges - as can be seen in Fig. 5 . This boundary condition also effectively models a fixed-edge support.

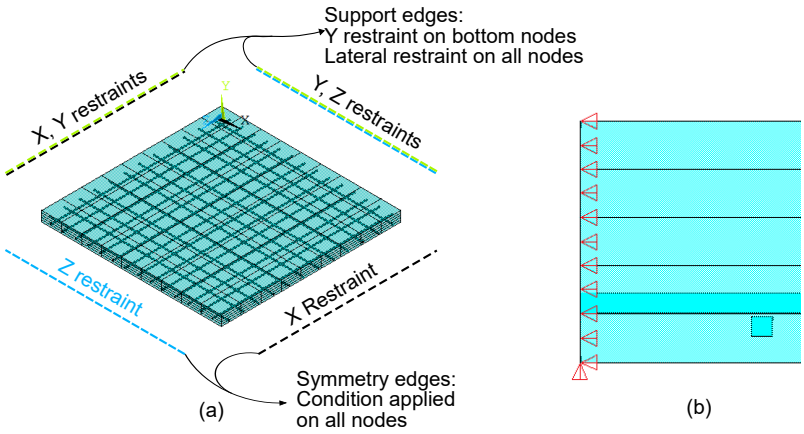

Figure 5: Boundary conditions for the quarter-model of the confined slabs. (a) Isometric view (b) support edge.

The model's excellent predictive capability extended to the 10 confined slab tests, where it accurately captured both the load-deflection curves and ultimate loads. This high degree of accuracy is quantified by a mean experimental-to-numerical ultimate load ratio of 1.00 and a standard deviation of 0.06. Table 2 summarizes the ultimate loads for all experimental and numerical results in this set.

Slab	Qu,exp (kN)	Qu,num (kN)	exp/num	Error (%)	ref.
3S1	748.11	724.53	1.03	3.3	
3S3	798.91	786.44	1.02	1.6	Keenan (1969)
3S4	741.18	706.10	1.05	5.0	
S1R	414.58	394.91	1.05	5.0	
S2R	375.67	389.07	0.97	3.4	
S3R	445.46	467.51	0.95	4.7	
S4R	405.26	368.26	1.10	10.0	Rankin et al. (1991)
S5R	398.50	411.93	0.97	3.3	
S6R	399.15	417.18	0.96	4.3	
S7R	385.64	421.31	0.92	8.5	

Table 2: Validation data for confined slabs.

2.4 Parametric study setup

To investigate the effect of realistic confinement, a typical nine-slab floor panel, shown in Fig. 6, was idealized. Two models of the central slab (S105) were developed for the study.

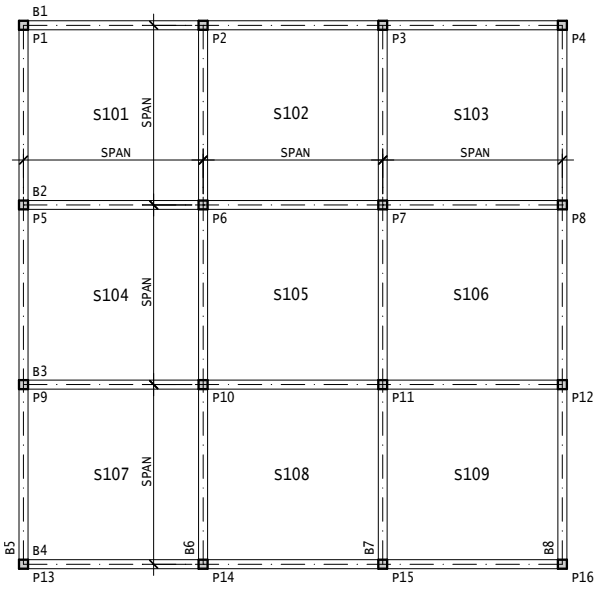

Figure 6: Structural plan of studied floor.

The unconfined model simulates a slab with fixed edges but without lateral confinement. The central slab was modeled in isolation. To achieve a fixed support condition that still allows for in-plane expansion, the horizontal displacements of all nodes along each support edge were coupled, forcing them to move together but not restraining the overall movement of the edge.

The confined model represents a more realistic scenario where in-plane restraint is provided by the surrounding floor. A quarter of the nine-slab floor plan was modeled. The central slab used the full nonlinear material model, while the adjacent slabs were modeled with a linear elastic material to provide confining stiffness in a computationally efficient manner.

Fig. 7 illustrates the models for both confined and unconfined slabs, with the boundary conditions defined as follows: blue lines represent rotationally fixed edges with coupled lateral displacement, allowing lateral movement; green lines represent simple vertical supports (rollers); and pink lines represent the model's symmetry boundaries.

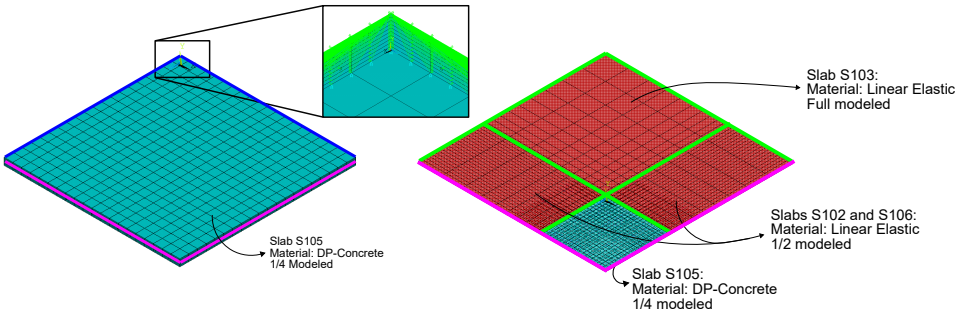

Figure 7: Modeling approach for the unconfined (left) and confined (right) parametric study cases.

3 RESULTS AND DISCUSSION

A parametric study involving 27 design cases was performed. The cases varied the slab span (4, 5, and 6 m), characteristic concrete strength (f_{ck} = 30, 40, and 50 MPa), and span-to-depth

ratio ($\lambda \approx 40$, 45, and 50) . Each design was analyzed with both the unconfined and confined models.

Table 3 presents a summary of slab design. For readability, the design cases were named according to the identifier LXX-Y-ZZ, where XX is the characteristic compressive strength of concrete (f_{ck}) in MPa, Y is the span in meters and ZZ is the slab's height in centimeters. Additionally, the symbol * was added to slabs that use the minimun reinforcement ratio prescribed by the code. A_s and A'_s are the reinforcements area on the span and supports, respectively.

Case	fck *(MPa)*	Span *(cm)*	Height *(cm)*	$\frac{\text{Span}}{\text{Height}}$	As *(cm²/m)*	As' *(cm²/m)*	Qu *(kN)*	Qc *(kN)*	$\frac{\text{Qc}}{\text{Qu}}$
L30-4-08	30	400	8	50	1.35	1.87	312.9	540.2	1.73
L40-4-08	40	400	8	50	1.34	1.85	339.6	600.5	1.77
L50-4-08	50	400	8	50	1.34	1.94	384.3	662.3	1.72
L30-5-10	30	500	10	50	1.63	2.32	514.4	849.0	1.65
L40-5-10	40	500	10	50	1.62	2.30	552.9	939.5	1.70
L50-5-10	50	500	10	50	1.62	2.29	554.6	1029.6	1.86
L30-6-12	30	600	12	50	1.96	2.82	729.1	1248.4	1.71
L40-6-12	40	600	12	50	1.95	2.79	789.2	1375.2	1.74
L50-6-12	50	600	12	50	1.94	2.78	850.7	1514.5	1.78
L30-4-09	30	400	09	44.4	1.17	1.64	350.7	704.0	2.01
L40-4-09*	40	400	09	44.4	1.19	1.79	408.0	817.2	2.00
L50-4-09*	50	400	09	44.4	1.38	2.07	444.6	898.5	2.02
L30-5-11	30	500	11	45.5	1.47	2.10	553.4	1050.0	1.90
L40-5-11	40	500	11	45.5	1.47	2.09	585.1	1168.0	2.00
L50-5-11*	50	500	11	45.5	1.57	2.36	639.4	1309.3	2.05
L30-6-13	30	600	13	46.2	1.81	2.62	799.3	1479.0	1.85
L40-6-13	40	600	13	46.2	1.80	2.60	834.0	1670.9	2.00
L50-6-13	50	600	13	46.2	1.80	2.66	903.7	1824.9	2.02
L30-4-10*	30	400	10	40	1.05	1.58	404.1	922.7	2.28
L40-4-10*	40	400	10	40	1.27	1.91	481.6	1063.0	2.21
L50-4-10*	50	400	10	40	1.48	2.21	575.6	1198.7	2.08
L30-5-12	30	500	12	41.7	1.35	1.94	588.4	1282.1	2.18
L40-5-12*	40	500	12	41.7	1.44	2.16	679.2	1474.3	2.17
L50-5-12*	50	500	12	41.7	1.68	2.51	818.8	1673.6	2.04
L30-6-15	30	600	15	40	1.59	2.31	916.9	2073.3	2.26
L40-6-15*	40	600	15	40	1.71	2.56	1057.9	2365.1	2.24
L50-6-15*	50	600	15	40	1.99	2.98	1210.1	2696.0	2.23

Table 3: Summary of the 27 design cases - data and results.

Table 3 presents the ultimate loads for the unconfined (Qu) and confined (Qc) models. The results demonstrate a significant increase in load capacity due to lateral confinement; on average, the confined slabs were 97% stronger than their unconfined equivalents. This finding confirms that stiffness from adjacent elements in a continuous floor system effectively induces compressive membrane action.

This strength enhancement is also reflected in the load-deflection curves, as shown for representative slabs in Fig. 8. The confined slabs exhibit a considerably stiffer post-cracking response and sustain significantly higher loads before failure.

Furthermore, the graph for slab L30-4-08 in Fig. 8 includes a curve for the theoretical case of perfect confinement, which assumes infinite axial stiffness from adjacent slabs. This comparison highlights that the slab's behavior is significantly influenced by the degree of confinement provided by the structural system.

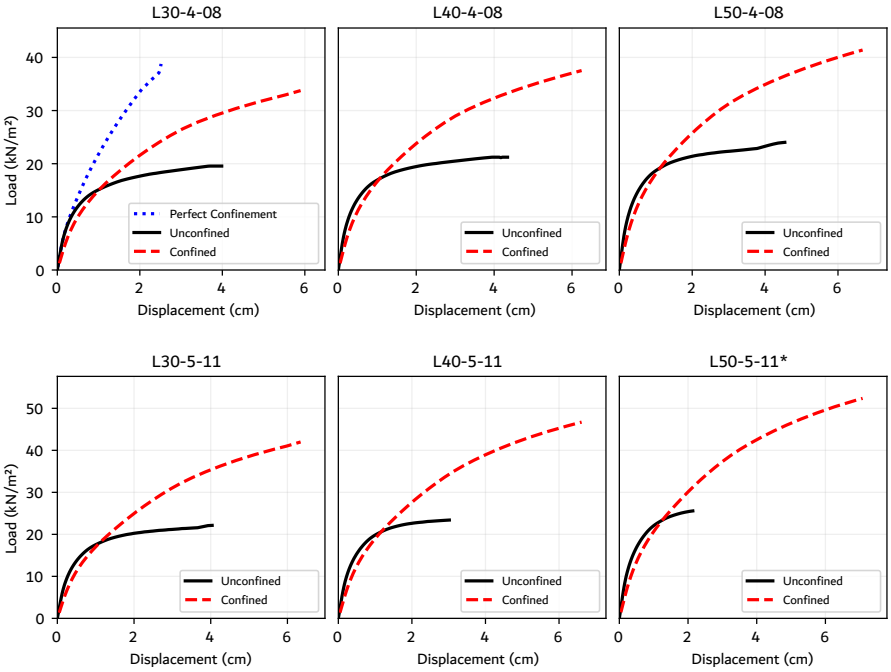

Figure 8: Displacement under load for some of the design cases.

The analysis of the parametric study revealed that the magnitude of this strength enhancement is not uniform across all designs. The largest gains were observed in slabs with shorter spans, higher concrete strengths (f_{ck}), and lower span-to-depth ratios (λ). This is because shorter, stiffer slabs develop higher in-plane forces; stronger concrete can sustain greater compressive stresses within the internal arch; and thicker, less slender slabs exhibit a more pronounced arching action.

The numerical model quantified the in-plane stiffness from adjacent slabs at approximately 1.2 times the target slab's axial stiffness, indicating strong lateral confinement.

4 CONCLUSIONS

This paper detailed the development, validation, and application of a 3D finite element model for simulating compressive membrane action in reinforced concrete slabs. The following conclusions were drawn from the study:

The developed numerical model, which uses SOLID186 elements with a Drucker-Prager Concrete material model and embedded REINF264 reinforcement, was successfully validated against a comprehensive set of 22 experimental tests, demonstrating its capability to accurately predict the ultimate load and deformation behavior of both unconfined and laterally confined RC slabs.

The explicit inclusion of lateral restraint from adjacent floor slabs in the model resulted in a substantial increase in the predicted ultimate load capacity. The average strength gain was 97%, nearly doubling the capacity compared to slabs modeled without in-plane confinement.

Compressive membrane action was shown to significantly improve the post-cracking stiffness of the slabs, leading to a more robust structural response with reduced deflections at high load levels.

The parametric study identified that the strength enhancement from membrane action is most pronounced in slabs with shorter spans, lower slenderness ratios, and higher concrete compres-

sive strengths.

The findings confirm that compressive membrane action is a powerful strength-enhancing mechanism inherent in continuous slab systems. Accounting for this effect in design could lead to more accurate safety assessments and more economical use of materials.

Future work could involve extending the validated model to investigate the influence of other parameters, such as flexible support conditions, slab openings, and punching shear behavior. Furthermore, the insights from an expanded parametric study could be used to develop simplified design recommendations, allowing practitioners to more readily account for compressive membrane action in routine design.

REFERENCES

Abdul-Wahab H.M.S. and Khalil M.H. Rigidity and strength of orthotropic reinforced concrete waffle slabs. *Journal of Structural Engineering*, 126(22):219–227, 2000. ISSN 0733-9445, 1943-541X. http://doi.org/10.1061/(ASCE)0733-9445(2000)126:2(219).

ABNT. Nbr6118: Projeto de estruturas de concreto. 2023.

ANSYS. *Ansys Mechanical APDL Guide*. Ansys, Inc., 2023.

Christiansen K. et al. The effect of membrane stresses on the ultimate strength of the interior panel in a reinforced concrete slab. *The Structural Engineer*, 41(8):261–265, 1963.

FIB. *Model Code for Concrete Structures 2010*. Fédération Internationale du Béton, 2010.

Geymayer H.G. and McDonald J.E. *Influence of Reinforcing Details on Yield Line Pattern and Ultimate Load-carrying Capacity of Reinforced Concrete Slabs*. 1967.

Gomes R.B., Campos C.D.O., Rocha A.P.D., and Melo G.S. Reforço em lajes de concreto armado. *REEC - Revista Eletrônica de Engenharia Civil*, 4(22), 2012. ISSN 2179-0612. http://doi.org/10.5216/reec.v4i2.19838.

Keenan W.A. *Strength and Behavior of Restrained Reinforced Concrete Slabs under Static and Dynamic Loadings*. Naval Civil Engineering Laboratory, 1969.

Liebenberg A. *Arch action in concrete slabs*, volume 40. National Building Research Institute, Council for Scientific and Industrial, 1966.

Okleston A.J. Loading tests on the floor systems of a reinforced concrete building. *The South African Institution of Civil Engineers*, 1956.

Park R. The ultimate strength and long-term behaviour of uniformly loaded, two-way concrete slabs with partial lateral restraint at all edges. *Magazine of Concrete Research*, 16(4848):139–152, 1964. ISSN 0024-9831, 1751-763X. http://doi.org/10.1680/macr.1964.16.48.139.

Pires E.F. *Comportamento e Desempenho do Reforço à Flexão de Lajes de Concreto Armado através do Aumento da Seção na Região Comprimida*. Dissertação de mestrado, Universidade Federal de Minas Gerais, Belo Horizonte, 2003.

Rankin B., Long A.E., Niblock R.A., and Skates A.S. Compressive membrane action strength enhancement in uniformly loaded, laterally restrained slabs. *The Structural Engineer*, 69(1616), 1991.

Taylor R., Maher D.R.H., and Hayes B. Effect of the arrangement of reinforcement on the behaviour of reinforced concrete slabs. *Magazine of Concrete Research*, 18(5555):85–94, 1966. ISSN 0024-9831, 1751-763X. http://doi.org/10.1680/macr.1966.18.55.85.

Zhu Y.J., Zhou M., Zhu J.M., and Nie X. Analytical models for load capacities of variable thickness reinforced concrete slabs considering compressive membrane action and boundary effects. *Engineering Structures*, 246, 2021. ISSN 01410296. http://doi.org/10.1016/j.engstruct.2021.113067.